

Enhanced Accuracy of Force Application for AFM Nanomanipulation Using Nonlinear Calibration of Optical Levers

Hui Xie, *Member, IEEE*, Julien Vitard, Dogan Sinan Haliyo, and Stéphane Régnier

Abstract—The atomic force microscope (AFM) has been widely used as a nano-effector with a function of force sensing to detect interaction forces between an AFM tip and a sample, thereby controlling the process of the nanomanipulation. However, both the extent and accuracy of force application are significantly limited by the nonlinearity of the commonly used optical lever with a nonlinear position-sensitive detector (PSD). In order to compensate the nonlinearity of the optical lever, a nonlinear calibration method is presented. This method applies the nonlinear curve fit to a full-range position-voltage response of the photodiode, obtaining a continuous function of its voltage-related sensitivity. Thus, interaction forces can be defined as integrals of this sensitivity function between any two responses of photodiode voltage outputs, instead of rough transformation with a single conversion factor. The lateral position-voltage response of the photodiode, a universally acknowledged puzzle, was directly characterized by an accurately calibrated force sensor composed of a tipless piezoresistive microcantilever and corresponding electronics, regardless of any knowledge of the cantilevers and laser measuring system. Experiments using a rectangular cantilever (normal spring constant 0.24 N/m) demonstrated that the proposed nonlinear calibration method restrained the sensitivity error of normal position-voltage responses to 3.6% and extended the force application range.

Index Terms—Atomic force microscope (AFM), force calibration, nanomanipulation, nonlinearity compensation, optical lever.

I. INTRODUCTION

ATOMIC FORCE MICROSCOPE (AFM), brought into the world more than two decades ago [1], has been proved to be a significant and popular tool for various application of scientific and industrial interest. As an important application domain of AFM, AFM based nanomanipulation made a great progress in recent years. Various AFM based nanomanipulation systems and manipulation schemes have been developed [2]–[11]. In order to facilitate the nanomanipulation, haptic devices and virtual reality interfaces were introduced into the AFM based nanomanipulation systems [12], [13], thereby enabling an operator to directly interact with the real nano world and overcoming the inherent

limitation of the AFM nanomanipulation, without a real time visual feedback to control the manipulation process. Augmented reality systems brought us further development by updating the local virtual environment using real-time feedback of tip-nano world interaction [14], [15]. Employing the same interface, operators can further monitor real-time changes of the nano environment through a movie-like AFM image [16]. All in all, haptics and visualization provide us friendly interfaces to easily manipulate nano objects.

However, highly precise position control of the AFM scanning stage and accurate detection of interaction forces between the AFM tip and nano objects or nano environment are prerequisite to a successful nanomanipulation. Method and models were developed to compensate positioning errors in the AFM caused by drift, creep, hysteresis, and other inherent nonlinearities [17], [18], aiming to overcome the spatial uncertainty and manipulate particles with sizes that are on the order of 10 nm. In most commercial AFM, the interaction forces between the AFM tip and nano objects are detected by an optical lever, which mainly consists of a laser and a position-sensitive detector (PSD) [19]. A Quadrant photodiode is widely used as a PSD to measure the normal force, simultaneously the lateral force from recording differences among its four segments and converting the corresponding signals into voltage outputs. Unfortunately, the limited linear range of the optical lever reduces the usable range and decreases the accuracy of the force application, especially when a soft cantilever with a small spring constant is used. The calibration and nonlinearity compensation of the force application are therefore most necessary for the accurate nanomanipulation. A robust approach to obtain a nonlinear expression of the displacement-voltage response using third-order polynomial fit was developed [20], reducing the systematic error from 50% to 5% on the sensitivity of the normal force response. However, the lateral nonlinearity of force application has been expected to be characterized.

In order to calculate the absolute values of normal and lateral forces using measured AFM voltage signals, normally it is necessary to know the accurate value of the spring constant of the cantilever and the sensitivity of the optical lever. A number of methods have been developed for the normal spring constant calibration of the cantilever [21], one method most commonly adopted was developed by Cleveland *et al.* who utilized frequency shifts caused by the known mass loaded on the free end of the cantilever [22]. The normal force applied to the tip can be simply calculated by multiplying the vertical deflection of the cantilever to its spring constant. Therefore, the normal force

Manuscript received December 11, 2007; revised February 1, 2008; accepted February 5, 2008. Published July 16, 2008 (projected). This work was supported in part by the European Project NANORAC under Grant STRP 013680. The associate editor coordinating the review of this manuscript and approving it for publication was Prof. Michael Schoening.

The authors are with the Institut des Systèmes Intelligents et Robotique, Université Pierre et Marie Curie /CNRS, 92265 Fontenay-Aux-Roses, France (e-mail: xie@robot.jussieu.fr; vitard@robot.jussieu.fr; haliyo@robot.jussieu.fr; regnier@robot.jussieu.fr).

Color versions of one or more of the figures in this paper are available online at <http://ieeexplore.ieee.org>.

Digital Object Identifier 10.1109/JSEN.2008.920722

conversion factor can be easily experimentally determined. In contrast, the lateral force calibration is more challenging to the normal calibration. Generally, two kinds of methods are commonly used: two-step methods [23], [24] and direct methods [25]–[27]. The two-step method involves the calibration of the torsional spring constant of the cantilever and the measurement of the lateral photodiode response. This method is not straightforward and is limited in application. The main reason is that the lateral sensitivity of the photodiode is difficult to determine because it should be significantly reduced due to the lateral contact stiffness between the tip and the sample [24], [25], which is often comparable to the lateral stiffness of the cantilever and its tip [28], [29].

The emphasis in this paper is the calibration and compensation for force application of the AFM based nanomanipulation system. For the lateral calibration, we present a new method to calibrate the lateral force measurement in atomic force microscope using a commercially available, accurately calibrated piezoresistive force sensor, which consists of a piezoresistive cantilever and accompanying electronics, providing a force standard for the lateral force calibration. During the force calibration, full range of the force-voltage data of normal and lateral application was recorded for the nonlinearity compensation of the optical lever. Compensation results provide a means that allows the accurate force application within the full detection range of optical lever during the manipulation.

This paper is organized as follows. Section II simply describes the AFM based nanomanipulation system. In Section III, methods for the normal and lateral force calibration are proposed. Nonlinear compensation of the force applications are discussed in Section IV. Section V presents conclusions.

II. AFM BASED NANOMANIPULATION SYSTEM

The AFM based nanomanipulation system with an augmented virtual reality is equipped with a nanopositioning stage with a maximum range of $50 \mu\text{m} \times 50 \mu\text{m}$ on X - Y axes and $12 \mu\text{m}$ on Z axis. An optical microscope (Olympus BX50WI with $20\times$ and $100\times$ objectives) is used to locate the laser spot on the cantilever and select the interested area for manipulation. The augmented reality consists of a PC based virtual environment and a haptic device (Virtuose 3D15-25, designed by CEA of France. Its kinematics allows 6 DOF movements with 5 N continuous force and 15 N maximum force feedbacks on 3 axes, providing 25 cm cube in workspace). These two subsystems are connected by ethernet. When a user manipulates the haptic device, generated position commands are transferred via the haptic controller to the coupled virtual nano-objects. The eXtended Dynamical Engine (XDE) is employed to compute the occurring interactions in the mechanical model under the simulated environment. The augmented reality system is designed in such a way that haptic control and vision computation run on different processing loops (30 Hz in vision corresponding to the human visual perception for the graphical loop and 1 kHz for the force feedback). Combining with the simulated, decoupled normal and lateral forces from the cantilever tip, the augmented reality provides the user real forces feel and a real-time visual display in the simulated environment during the nanomanipulation.

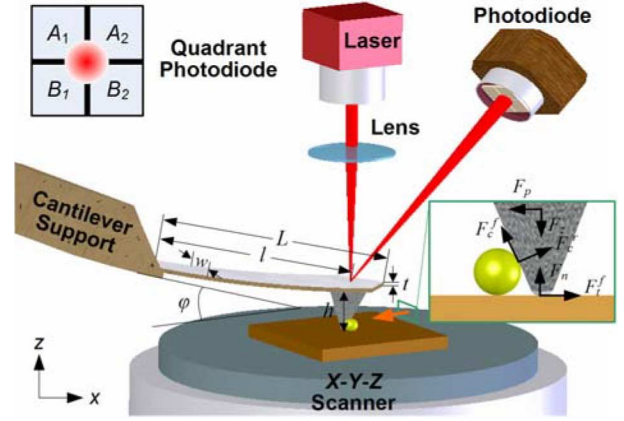


Fig. 1. Optical arrangement in a typical AFM. A quadrant photodiode is used to detect the normal and torsional signals. A cantilever, mounted with an angle ϕ to the sample surface, is built in at one end, free at the other end assumed to deform in the linear elastic range. L , l , w , t , and h are the length, effective length, width, thickness, and tip height of the cantilever, respectively.

III. CALIBRATION OF THE FORCE APPLICATION

A. Scheme for the Force Application

The crucial element in an AFM is a device for measuring the force applied on the tip due to its interaction with the sample. The commonly used optical lever, mainly composed of a laser and a PSD, is believed to be more sensitive and reliable detection device than others [30], [31]. As depicted in Fig. 1, this method makes use of a photodiode consisting of two or four closely jointed segments to detect nanoscale deflection of the cantilever. A fairly well focused laser beam is reflected from the backside of the cantilever and then reflected off a mirror before reaching the photodiode. Forces applied on the tip result in deflections (corresponding angular deflection θ) of the cantilever, causing unbalanced signal output of the photodiode segments. These signals are further amplified by external electronics and then are employed as input signals for the forces feedback during the manipulation. For example, in our system, a quadrant photodiode is used to detect the normal and torsional signals by the electronics output $V_n = (V_{A1} + V_{A2}) - (V_{B1} + V_{B2})$ and $V_l = (V_{A1} + V_{B1}) - (V_{A2} + V_{B2})$, respectively. In order to convert these signals into forces, one need to calibrate the normal and lateral force factors β and α , by which the corresponding forces F_n and F_l are given by

$$F_n = \beta \times \Delta V_n \quad (1)$$

$$F_l = \alpha \times \Delta V_l \quad (2)$$

where each ΔV represents the change in the respective signal due to an applied force in the respective direction relative to any offset of the signal captured when no force is applied on the cantilever. The main aim of this section is to calibrate the normal and lateral force factors β and α .

B. Normal Force Calibration

In experiments, an AFM cantilever with a rectangular cross section and a normal force constant of 0.24 N/m was used: ContAL (NANOWORD). Although dimensions of the

TABLE I
CALIBRATION RESULTS OF THE NORMAL AND LATERAL FORCE APPLICATION

$t(\mu\text{m})$	$f_0(\text{kHz})$	$k_n(\text{N/m})$	$k_l(\text{N/m})$	$\beta(\mu\text{N/V})$	$\alpha(\mu\text{N/V})$
2.14	13.30	0.24	74.90	0.47 ± 0.02	14.85 ± 1.66

cantilever were provided by the manufacture, the optical microscope was used to measure the cantilever's dimensions ($L = 466 \mu\text{m}$, $l = 455 \mu\text{m}$, $w = 51.4 \mu\text{m}$, and $h = 16.5 \mu\text{m}$). In our experiment, forced oscillation was employ to determine the thickness t of the cantilever based on its natural frequency. For the Euler-Bernoulli beam, if we know the resonant frequencies of the cantilevers, the thickness t can be obtained by [32]

$$t = \frac{\omega_n}{K_n^2} \sqrt{\frac{12\rho}{E}} \quad (3)$$

where K_n is the wave number on the cantilever, ω_n is the n th flexural resonant frequency. If $n = 1$, then $K_n L = 1.8751$, in which L is the length of the cantilever. Its normal and lateral spring k_n and k_l can be calculated by

$$k_n = \frac{Ewt^3}{4L^3} \quad (4)$$

$$k_l = \frac{Gwt^3}{3L(h + \frac{t}{2})^2} \quad (5)$$

where w and t are the width and thickness of the cantilever, respectively. When the normal spring constant k_n is determined, the normal force can be calculated by

$$\beta = \frac{k_n \delta_n}{\Delta V_n} \quad (6)$$

where δ_n is the deflection of the cantilever, ΔV_n is the corresponding voltage output of the photodiode.

The next step is to calibrate the normal force factor. In our experiment, the cantilever's tip contacted with a glass loading button. The Z nanostage was employed for the precisely loading on the cantilever tip. After slightly touching the loading button, the Z nanostage was moved upward with an increment of 5 nm in the frequency of 1 Hz. After 20 complete calibration cycles, the normal force factor β of this cantilever was calibrated as $0.47 \mu\text{N/V}$ using a linear fit 40% of the total range of the photodiode response [see Fig. 5(a)]. The calibration results are shown in Table I.

C. Lateral Force Calibration

1) *Calibration of the Piezoresistive Force Sensor:* The piezoresistive cantilever (Nascatec GmbH, Germany) and accompanying electronics are commercially available in our work. Microscopy images of the piezoresistive are shown in Fig. 2. Dimensions of the piezoresistive cantilever were measured as $525.8 \mu\text{m}$ in length and with an average width of $152.7 \mu\text{m}$. The top view Fig. 2(b) shows that the clamping end of the piezoresistive cantilever has a step shape with a difference of $12.5 \mu\text{m}$ on the width and a hole with a length of $15 \mu\text{m}$ on square. Therefore it is not convenient to directly calculate its normal spring constant using the beam mechanics. Therefore,

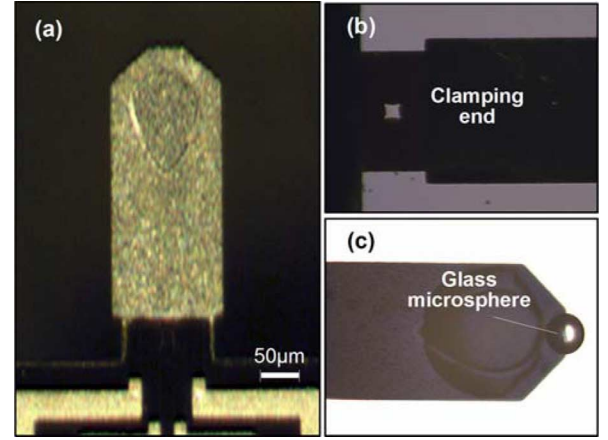


Fig. 2. Optical microscopy images of the piezoresistive cantilever used in the lateral force calibration. (a) Top image of the piezoresistive cantilever. (b) Shape of the clamping end of the piezoresistive cantilever is with a step shape and a hole in its middle. (c) Image obtained after a glass microsphere attached on the tip of the piezoresistive cantilever.

the piezoresistive cantilever stiffness k_p was calibrated using Cleveland's mass loading method [22]

$$k_p = (2\pi)^2 \frac{M_1}{\left(\frac{1}{v_1^2} - \frac{1}{v_0^2}\right)} \quad (7)$$

where v_0 is the unloaded resonant frequency and v_1 is the resonant frequency with a loaded mass M_1 . We used six glass microspheres with diameters from $25.6 \mu\text{m}$ to $64.4 \mu\text{m}$ measured under the optical microscope, and used a glass density of 2.4 g/cm^3 . The glass microspheres were placed on the free end of the piezoresistive cantilever and their centers were also measured by the optical microscope for stiffness compensation due to position errors [in Fig. 2(c)] using

$$k_p = k_d \left(\frac{l_d}{L_p}\right)^3 \quad (8)$$

where k_d is the measured spring constant as a glass microsphere with its center located at l_d from the base of the piezoresistive cantilever which has an overall length L_p , k_p is then the spring constant if the same glass microsphere is placed at the very end of the piezoresistive cantilever.

The stiffness of the piezoresistive cantilever was calibrated at $k_p = 18.209 \pm 0.471 \text{ N/m}$. In the force sensitivity calibration of the piezoresistive sensor, it was mounted horizontally on a 3 DOF platform. A Z nanostage (resolution 1.8 nm) with an attached glass substrate was used for the displacement increments during the calibration. A program was used to control the motion of the nanostage with a fixed increment (20 nm in our experiment) while the voltage output V_p of the electronics was recorded. It was found that the displacement of the piezoresistive cantilever tip was approximately $5.7 \mu\text{m}$ across the full range of the piezoresistive force sensor output. After 20 complete loading/unloading calibration cycles, A piezoresistive force sensitivity $S_p = 10.361 \pm 0.267 \mu\text{N/V}$ was achieved.

2) *Lateral Calibration of the AFM Cantilever:* Once the piezoresistive force sensor has been calibrated, it was used as a force standard to determine the conversion factors α of the AFM cantilevers. The piezoresistive cantilever was mounted

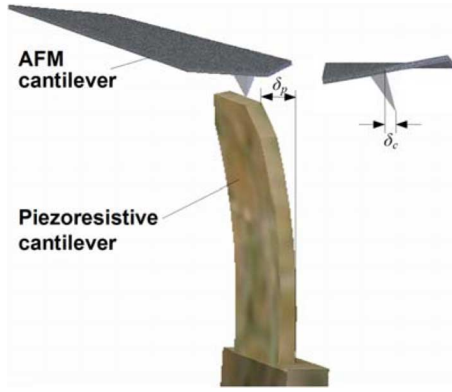


Fig. 3. Scheme of the experimental configurations for the calibration of the AFM with a piezoresistive force sensor. The deflection of the piezoresistive and testing cantilever are δ_p and δ_c , respectively.

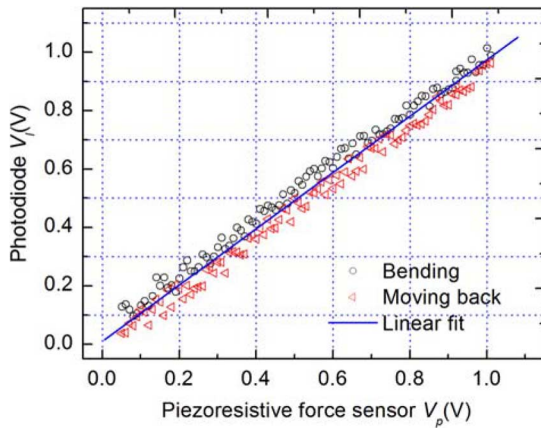


Fig. 4. Example of photodiode voltage outputs plotted versus voltage output of the piezoresistive force sensor. Symbols of the red open triangles and black open circles show data obtained from the cases of bending and moving back. The straight, blue line is the linear fit of the corresponding data using the least square method.

vertically on the AFM stage along its longitudinal axis (see Fig. 3). In this case, the tip of the testing cantilever contacts the top end of the piezoresistive cantilever in the lateral calibration. After the AFM cantilever was brought into contact with the top surface of the piezoresistive cantilever, the contact mode was used to scan the top side edge to identify its center point. Then the AFM cantilever was moved $2 \mu\text{m}$ away from the scanned side edge. In order to ensure the AFM tip was reliably in contact with the top side edge, the AFM cantilever was moved down with a displacement $\Delta h = 0.5 - 0.8 \mu\text{m}$ before being moved back to contact with the loading location.

The loading location is on the top edge of the piezoresistive force sensor, so the lateral force conversion factor α can be simplified obtained by

$$\alpha = \frac{F_t}{V_l} = \frac{S_p V_p}{V_l} \quad (9)$$

where V_p and V_l are voltage outputs of the piezoresistive force sensor and the photodiode, respectively.

Each cantilever was used to laterally bend the piezoresistive cantilever for ten times. For each time the lateral force conversion factor was calculated and as outlined in Fig. 4, in which the symbols of the triangles and circles show data obtained from the

cases of bending and moving back, respectively. The straight line is the linear fit of the corresponding data using the least square method and its gradient was used to calculate α via (9). Then value of the lateral force conversion factors α was averaged from ten times of experimental results.

For the proposed method, we need to take into account errors generated by the calibration of the piezoresistive cantilever as well as those from the lateral force calibration of AFM cantilevers. The errors in these measurements of S_p , V_p , V_l are of the order of 11%, 0.02 V, and 0.02 V, also considering the error generated from displacement Δh , the maximum overall error for the calibration of the lateral conversion factor α using the proposed method is 12.3%, which largely depends on the uncertainty of S_p . If an absolute force standard is used to calibrate the piezoresistive force sensor, an error of less than 6% can be expected. The piezoresistive force sensor has several attractive features. The most significant fact is that it can provide a force standard for the direct calibration of the lateral force conversion factors without any knowledge of the photodiode, or cantilever shape, dimensions and physical properties, thereby overcoming almost all the difficulties in the calibration of the lateral force measurement. The experimental results of the normal and lateral calibration are summarized in Table I.

IV. COMPENSATION OF THE FORCE CALIBRATION

A. Traditional Force Calibration

Various literatures analyzed and discussed the characterization of the sensitivity of the optical lever [33]–[35]. The sensitivity of the optical lever can be enhanced by increasing the intensity of the laser beam or by decreasing the beam divergence. Moreover, during the force calibration, the sensitivity of the optical lever has strong dependences on the position of the laser spot relative to the center of the PSD and geometry of the optical path [24], [36]. Main causes that introduce the nonlinearities are the shape and intensity distribution of the laser spot on the PSD [37], which limit the range of real force application in AFM, especially when a very “soft” cantilever is used.

For the traditional force calibration of the AFM, the photodiode sensitivity S_{PSD} is considered as linear response to the force applied on cantilever’s tip by

$$S_{PSD} = \frac{V_{PSD} - V_{PSD}^0}{\delta_p} \quad (10)$$

where $\theta_n = 3/2lF_n/k_n$ and $S_{PSD}^n = 2l/3dV_{PSD}^n/d\delta_n$ are the voltage output of the photodiode before and after the force loading, δ_p is the tip deflection with a force loading.

Actually, the photodiode sensitivity S_{PSD} is not constant, that is the plot of the photodiode voltage output V_{PSD} versus the applied force is nonlinear. In fact, our experiments indicated that more than 200% variation in S_{PSD} is a function of the range and initial value of the photodiode voltage output. The most important factors that introduce the nonlinearity are the shape and intensity distribution of the laser spot. If the spot is near the center of the photodiode, the response is linear. When the spot deviates from the center of the photodiode, the nonlinearity becomes more obvious. The force/displacement-voltage response of the AFM therefore should be accurately calibrated in the full range of the photodiode.

B. Nonlinear Compensation of the Force Application

For the convenience of normal and lateral calibration, angular sensitivity S_{PSD} is used in our experiments, which is independent of the dimensions of the cantilevers and directly reveals the mechanism of the deflection measurement. The angular sensitivity S_{PSD} is defined as a ratio of the angular deflection of the cantilever and the photodiode voltage output. Thus, the normal photodiode sensitivity is $S_{PSD}^n = \Delta V_{PSD}^n / \theta_n$ and the lateral sensitivity $S_{PSD}^l = \Delta V_{PSD}^l / \theta_l$. Here, θ_n and θ_l are defined as the normal and lateral angular deflection of the cantilever.

The normal spring constant k_n connects the flexural deflection δ_n due to an applied normal force $F_n = k_n \delta_n$. So based on the beam mechanics, θ_n can be presented as

$$\theta_n = \frac{3 F_n}{2l k_n} \quad (11)$$

where l is the effective length of the cantilever. Therefore, if we know the continuous function of $S_{PSD}^l = dV_{PSD}^l / d\theta_l$, so can be determined by

$$S_{PSD}^n = \frac{2l}{3} \frac{dV_{PSD}^n}{d\delta_n}. \quad (12)$$

For a cantilever with rectangular cross section, the torsional angle θ_l related to the applied force F_l by

$$\theta_l = \frac{3F_l l (h + \frac{t}{2})}{Gwt^3} \quad (13)$$

where G is the shear modulus of the cantilever. Thus the lateral sensitivity of the photodiode can be also determined by

$$S_{PSD}^l = \frac{dV_{PSD}^l}{d\theta_l}. \quad (14)$$

Continuous functions of the normal and lateral sensitivities can be determined by the calibration and nonlinear fit of the position-voltage curves. Thus, in the actual application, the angular deflection of the cantilever can be obtained by

$$\theta_n = \int_{V_{PSD}^{n0}}^{V_{PSD}^{n1}} \frac{1}{S_{PSD}^n} dV_{PSD}^n \quad (15)$$

$$\theta_l = \int_{V_{PSD}^{l0}}^{V_{PSD}^{l1}} \frac{1}{S_{PSD}^l} dV_{PSD}^l \quad (16)$$

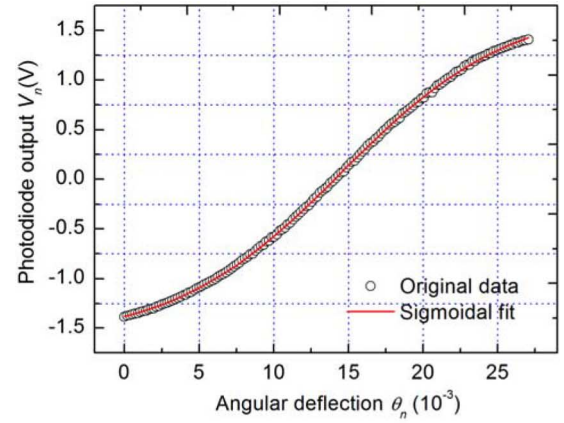
where the lower and upper limits are the initial and force deduced voltage outputs of the photodiode. Also the normal and lateral tip displacement can be calculated by

$$\delta_n = \frac{2l}{3} \theta_n \quad (17)$$

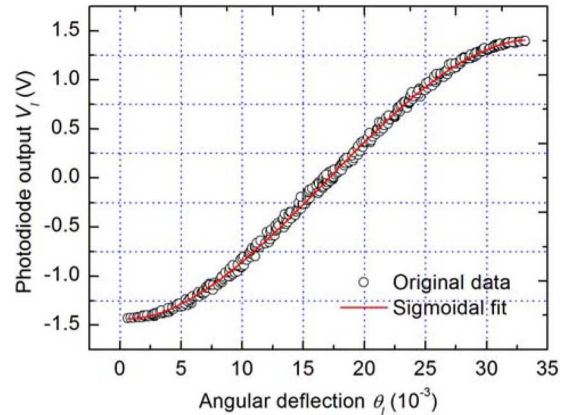
$$\delta_l = \theta_l \left(h + \frac{t}{2} \right). \quad (18)$$

In the actual application, the whole nonlinear calibration protocol can be carried as follows.

- 1) Set the initial voltage output (without force loading) of the photodiode near the lower point by adjusting the position of reflecting laser spot.
- 2) Record original force/position-voltage responses by the normal and lateral force calibration.



(a)



(b)

Fig. 5. Force calibration curves (V_{PSD}, θ) and Sigmoidal fitting results using the Dose response function. (a) Normal V_{PSD} versus θ_n response. (b) Lateral V_{PSD} versus θ_l response. All the responses are in almost the full range of the photodiode signal output. The open circle symbol represents the original data calculated from the force calibration results and the red line is the Sigmoidal fitting results.

- 3) Transform the force/position-voltage responses to voltage-angular sensitivity responses by (11) and (13) for normal and lateral cases, respectively.
- 4) Employ nonlinear fit voltage-angular sensitivity responses to obtain continuous functions of V_{PSD} and then calculate the angular sensitivity S_{PSD} by (12) and (14).
- 5) Calculate the angular deflection on the AFM using (15) and (16) for normal and lateral force, respectively. Then the applied forces on the AFM tip can be easily obtained.

C. Experimental Results

The experiments described below were performed on an AFM based nanorobotic system. The voltage range of the position detector, unlike ± 10 V of a common AFM, is ± 1.5 V because electronics with a lower ratio of signal amplifier is used. Nonetheless, the general approach can be widely applicable and the only difference is just the calibrated conversion parameters described in Table I.

Inspired by the sigmoidal shape of the V_{PSD} versus θ curves presented in Fig. 5, the method of Sigmoidal fit was employed to the normal and lateral voltage-angular sensitivity response

TABLE II
PARAMETERS OF THE SIGMOIDAL FIT

Calibration Type	A_1	A_2	θ_0	p
Normal	-1.62358	1.76318	14.55008	0.07663
Lateral	-1.61967	1.71585	16.98019	0.06446

(V_{PSD} , θ) in the experiments. The common Dose response function was used in the Sigmoidal fit by

$$V_{PSD} = A_1 + \frac{A_2 - A_1}{1 + 10^{(\theta_0 - \theta)p}} \quad (19)$$

where A_1 , A_2 , p , and θ_0 are the nonlinear fit parameters: lower limit, upper limit, slope, and the value of θ as half value of V_{PSD} . All the responses are in the almost full range of the photodiode signal output.

The next step is to calculate the inverse angular sensitivities of the photodiode, which can be obtained as the derivative of the Sigmoidal fit described in (19)

$$S_{PSD}^{-1} = \frac{d\theta}{dV_{PSD}} = \frac{(1 + \xi)^2}{(A_2 - A_1)\xi p \ln 10} \quad (20)$$

where $\xi = -(A_2 - V_{PSD})/(A_1 - V_{PSD})$.

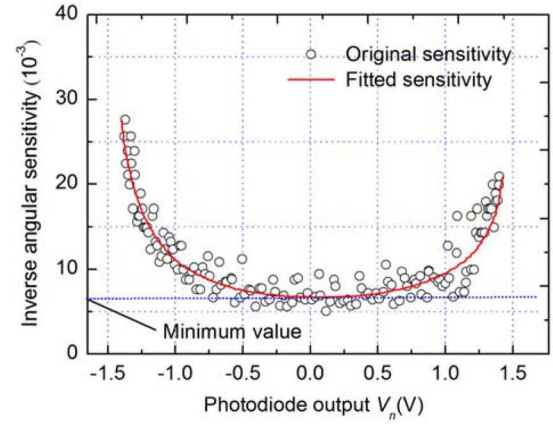
Thus we get a continuous function of the angular sensitivity S_{PSD} on the full range of photodiode voltage output V_{PSD} , rather than a single value. This function will be used to calculate the compensated normal and lateral angular deflections by (15) and (16) (rather than from (11) and (13), which assumes a linear transform between applied force and deflection with a single value of the sensitivity S_{PSD}), respectively. So a simple expression of the angular deflection between any two signal outputs V_{PSD}^0 and V_{PSD}^1 can be obtained by

$$\theta = -\frac{\ln |\xi|}{2.302585 \cdot p} \left| \frac{V_{PSD}^1}{V_{PSD}^0} \right|. \quad (21)$$

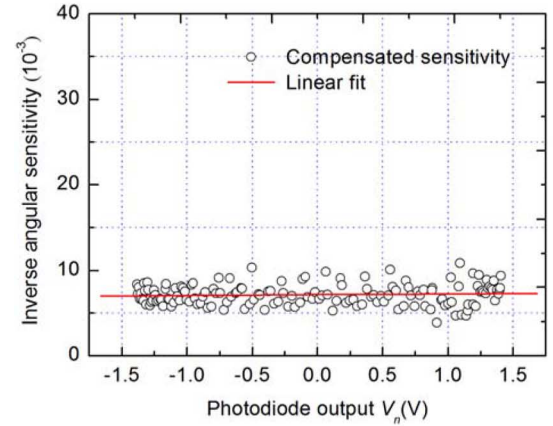
Voltage-angular deflection responses (V_{PSD} , θ) of the normal and lateral cases used for the calculation of the photodiode sensitivities S_{PSD} were obtained by the real force calibrations with a “soft” cantilever with a normal spring constant of 0.24 N/m. The Dose response function was used to fit the (V_{PSD} , θ) responses and fitting parameters are shown in Table II, which would be used to calibrate the sensitivity S_{PSD} via (21).

Sigmoidal fit results are shown in Fig. 5, including the force calibration curves (V_{PSD} , θ) (open circle) and fitting results using the Dose response function (red line). Fig. 5(a) shows the normal V_{PSD} versus θ_n response, and the lateral V_{PSD} versus θ_n response is presented in Fig. 5(b). All the responses are in the almost 95% full range of the photodiode signal output (± 1.43 V). For the lateral calibration, the angular deflection is calculated via (13) with the readout of the piezoresistive force sensor.

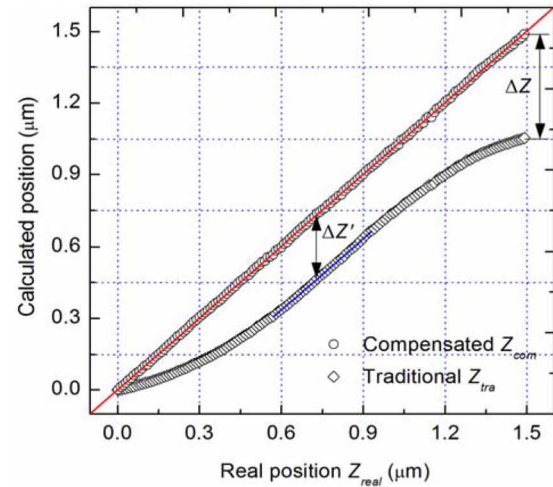
In order to further verify the proposed method for the nonlinearity compensation, an apparent sensitivity compensation experiment was evaluated using the response of the normal inverse S_{PSD} versus the normal voltage V_{PS} . Fig. 6(a) shows that more than 200% variation in normal S_{PSD} is the function in the full



(a)



(b)



(c)

Fig. 6. (a) Normal inverse sensitivity versus normal voltage as the slope $d\theta/dV_{PSD}$ of the normal (V_{PSD} , θ_n) response shown in Fig. 5(a). (b) Compensated normal inverse sensitivity using Sigmoidal fit of data shown in Fig. 6(a). The corresponding linear fit (the slope is 0.087) shows the nonlinearity is reduced from more than 200% to 3.6%. (c) Compensated position Z_{com} and traditional calibrated Z_{tra} versus real position Z_{real} recorded by the AFM stage. The slope of the linear fit of the compensated position curve is 0.9996.

range of the photodiode voltage output. The fitting sensitivity (red line) generated from the Sigmoidal fit is in accordance with the shape of the real sensitivity curve. The blue straight line, obtained from a linear fit of the bottom on the real sensitivity

curve, indicates that an inverse sensitivity 6.92×10^{-3} rad/V is the minimum value of this curve, presenting the highest sensitivity when the laser spot is near the center of the photodiode.

For easier representation, the results of the sensitivity compensation, the ratio of the real and the fitting sensitivity was multiplied by the minimum inverse sensitivity in Fig. 6(a), giving an apparent compensated sensitivity as shown in Fig. 6(b). The slope of the linear fit of the compensated sensitivity is 0.087 (red line), resulting in a variation of 3.6% in contrast with more than 200% before the compensation. The range of the force measurement was extended from 36% to 95% of the full range (within 5% minimum value of the sensitivity, the photodiode signal is in -0.5 V to $+0.58$ V, which represents 36% of the full range of ± 1.5 V), and the corresponding force application range improved from $0.25 \mu\text{N}$ to $0.69 \mu\text{N}$ of the cantilever with a spring constant of 0.24 N/m.

Fig. 6(c) shows the further comparison of the positions calculated from the traditional and the proposed method. The diamond symbol shows a nonlinear relationship between the calculated positions by traditional method Z_{tra} versus real position Z_{real} recorded by the AFM stage, resulting in an overall position error $\Delta Z = 0.434 \mu\text{m}$ (28.9% of the total displacement in the full range of the photodiode). The symbol of the circles displays an approximately straight line of compensated position Z_{com} with a gradient of 0.9996. Note that both plots have a same value of the linear fit near the center of the photodiode, where the position difference $\Delta Z'$ keeps constant due to the linear sensitivity in this area. The experiments results indicated that an excellent nonlinear fit obtained by the proposed method.

V. CONCLUSION

In order to obtain highly-precise force detection and extend the force application range of the AFM based nanomanipulation system, the normal and lateral force applications were accurately calibrated and the corresponding nonlinear sensitivities were well compensated by the proposed method. For the calibration of the lateral force, a new method, making use of an accurately calibrated piezo-force sensor composed of a tipless piezoresistive cantilever and corresponding electronics, was employed to determine the lateral force conversion factor. This method may be used to directly calibrate factor between the lateral force and the photodiode signal for cantilevers with a wide range of spring constant, regardless of their size, shape, material or coating effect, and any knowledge of the optical lever. A practicable approach was developed to compensate the sensitive nonlinearity of photodiode by calculating the cantilever deflection using the nonlinear fit of the sensitivity, which was achieved from the Sigmoidal fit of the normal and lateral force-voltage curves, thereby extending the effective force application range of the optical lever. The experimental results demonstrated that the sensitivity error of normal responses could be reduced from more than 200% to 3.6% and the range of the force application was extended.

ACKNOWLEDGMENT

The authors would like to thank D. Urma from CEA of France for her fruitful discussion about the augmented reality system and some corresponding material for the system description.

REFERENCES

- [1] G. Binning, C. F. Quate, and C. Gerber, "Atomic force microscope," *Phys. Rev. Lett.*, vol. 56, no. 9, pp. 930–933, Mar. 3, 1986.
- [2] J. A. Stroscio and D. M. Eigler, "Atomic and molecular manipulation with the scanning tunneling microscope," *Science*, vol. 254, no. 5036, pp. 1319–1326, 1991.
- [3] T. Junno, K. Deppert, L. Montelius, and L. Samuelson, "Controlled manipulation of nanoparticles with an atomic force microscope," *Appl. Phys. Lett.*, vol. 66, no. 26, pp. 3627–3629, Jun 26, 1995.
- [4] M. Martin, L. Roschier, P. Hakonen, U. Parts, M. Paalanen, B. Schleicher, and E. I. Kauppinen, "Manipulation of ag nanoparticles utilizing noncontact atomic force microscopy," *Appl. Phys. Lett.*, vol. 73, no. 11, pp. 1505–1507, Sep. 14, 1998.
- [5] R. Resch, A. Bugacov, C. Baur, B. E. Koel, A. Madhukar, A. A. G. Requicha, and P. Will, "Manipulation of nanoparticles using dynamic force microscopy: Simulation and experiments," *Appl. Phys. Mater. Sci. Process.*, vol. 67, no. 3, pp. 265–271, Sep. 1, 1998.
- [6] C. Baur, A. Bugacov, B. E. Koel, A. Madhukar, N. Montoya, T. R. Ramachandran, A. A. G. Requicha, R. Resch, and P. Will, "Nanoparticle manipulation by mechanical pushing: Underlying phenomena and real-time monitoring," *J. Inst. Phys. Nanotechnol.*, vol. 9, no. 4, pp. 360–364, 1998.
- [7] R. Resch, D. Lewis, S. Meltzer, N. Montoya, B. E. Koel, A. Madhukar, A. A. G. Requicha, and P. Will, "Manipulation of gold nanoparticles in liquid environments using scanning force microscopy," *J. Ultramicrosc.*, vol. 82, no. 1–4, pp. 135–139, Feb. 2000.
- [8] S. Decossas, F. Mazen, T. Baron, G. Brémond, and A. Souifi, "Atomic force microscopy nanomanipulation of silicon nanocrystals for nanodevice fabrication," *J. Inst. Phys. Nanotechnol.*, vol. 14, no. 12, pp. 1272–1278, 2003.
- [9] J. Hu, Y. Zhang, B. Li, H. B. Gao, U. Hartmann, and M. Q. Li, "Nanomanipulation of single DNA molecules and its applications," *Surf. Interface Anal.*, vol. 36, no. 2, pp. 124–126, 2004.
- [10] P. Dieska and I. Stich, "Nanomanipulation using only mechanical energy," *Phys. Rev. Lett.*, vol. 95, no. 12, 2005.
- [11] S. Kawaia and H. Kawakatsu, "Mechanical atom manipulation with small amplitude dynamic force microscopy," *Appl. Phys. Lett.*, vol. 89, no. 2, 2006.
- [12] S. G. Kim and M. Sitti, "Task-based and stable telenanomanipulation in a nanoscale virtual environment," *IEEE Trans. Autom. Sci. Eng.*, vol. 3, no. 3, pp. 240–247, Jul. 2006.
- [13] M. Sitti and H. Hashimoto, "Teleoperated touch feedback from the surfaces at the nanoscale: Modeling and experiments," *IEEE/ASME Trans. Mechatron.*, vol. 8, no. 2, pp. 287–298, Jun. 2003.
- [14] G. Y. Li, N. Xi, M. M. Yu, and W. K. Fung, "Development of augmented reality system for afm-based nanomanipulation," *IEEE/ASME Trans. Mechatron.*, vol. 9, no. 2, pp. 358–365, Jun. 2004.
- [15] W. Vogl, B. K. L. Ma, and M. Sitti, "Augmented reality user interface for an atomic force microscope-based nanorobotic system," *IEEE Trans. Nanotechnol.*, vol. 5, no. 4, pp. 397–406, Jul. 2006.
- [16] G. Y. Li, N. Xi, H. P. Chen, C. Pomeroy, and M. Prokos, "Videolized" atomic force microscopy for interactive nanomanipulation and nanoassembly," *IEEE Trans. Nanotechnol.*, vol. 4, no. 5, pp. 605–615, Sep. 2005.
- [17] B. Mokaberi and A. A. G. Requicha, "Drift compensation for automatic nanomanipulation with scanning probe microscopes," *IEEE Trans. Autom. Sci. Eng.*, vol. 3, no. 3, pp. 199–207, Jul. 2006.
- [18] B. Mokaberi and A. A. G. Requicha, "Compensation of scanner creep and hysteresis for AFM nanomanipulation," *IEEE Trans. Autom. Sci. Eng.*, vol. 5, no. 2, pp. 197–206, Apr. 2008.
- [19] G. Meyer, "Novel optical approach to atomic force microscopy," *Appl. Phys. Lett.*, vol. 53, no. 25, pp. 2400–2402, 1988.
- [20] E. C. C. M. Silva and K. J. V. Vliet, "Robust approach to maximize the range and accuracy of force application in atomic force microscopes with nonlinear position-sensitive detectors," *J. Inst. Phys. Nanotechnol.*, vol. 17, no. 22, pp. 5525–5530, 2006.
- [21] N. A. Burnham, X. Chen, C. S. Hodges, G. A. Matei, E. J. Thoreson, C. J. Roberts, M. C. Davies, and S. J. B. Tandler, "Comparison of calibration methods for atomic-force microscopy cantilevers," *J. Inst. Phys. Nanotechnol.*, vol. 14, no. 1, pp. 1–6, Jan. 1, 2003.
- [22] J. P. Cleveland, S. Manne, D. Bocek, and P. K. Hansma, "A nondestructive method for determining the spring constant of cantilevers for scanning force microscopy," *Rev. Sci. Instrum.*, vol. 64, no. 2, pp. 403–405, Feb. 1993.

- [23] R. G. Cain, S. Biggs, and N. W. Page, "Force calibration in lateral force microscopy," *J. Colloid Interface Sci.*, vol. 227, no. 1, pp. 55–65, Jul. 1, 2000.
- [24] R. J. Cannara, M. Eglin, and R. W. Carpick, "Lateral force calibration in atomic force microscopy: A new lateral force calibration method and general guidelines for optimization," *Rev. Sci. Instrum.*, vol. 77, no. 5, pp. 053701–1053701, 2006.
- [25] D. F. Ogletree, R. W. Carpick, and M. Salmeron, "Calibration of frictional forces in atomic force microscopy," *Rev. Sci. Instrum.*, vol. 67, no. 9, pp. 3298–3306, Sep. 1996.
- [26] M. Varenberg, I. Etsion, and G. Halperin, "An improved wedge calibration method for lateral force in atomic force microscopy," *Rev. Sci. Instrum.*, vol. 74, no. 7, pp. 3362–3367, 2003.
- [27] W. H. Liu, K. Bonin, and M. Guthold, "Easy and direct method for calibrating atomic force microscopy lateral force measurements," *Rev. Sci. Instrum.*, vol. 78, no. 6, pp. 063707–1063707, 2007.
- [28] R. W. Carpick, D. F. Ogletree, and M. Salmeron, "Lateral stiffness: A new nanomechanical measurement for the determination of shear strengths with friction force microscopy," *Appl. Phys. Lett.*, vol. 70, no. 12, pp. 1548–1550, 1997.
- [29] M. A. Lantz, S. J. O'shea, A. C. F. Hoole, and M. E. Welland, "Lateral stiffness of the tip and tip-sample contact in frictional force microscopy," *Appl. Phys. Lett.*, vol. 70, no. 8, pp. 970–972, 1997.
- [30] G. Meyer and N. M. Amer, "Novel optical approach to atomic force microscopy," *Appl. Phys. Lett.*, vol. 53, no. 12, pp. 1045–1047, Sep. 19, 1988.
- [31] S. Alexander, L. Hellemans, O. Marti, J. Schneir, V. Elings, and P. K. Hansma, "An atomic-resolution atomic-force microscope implemented using an optical lever," *J. Appl. Phys.*, vol. 65, no. 1, pp. 164–167, Jan. 1, 1989.
- [32] D. A. Mendels, M. Lowe, A. Cuenat, M. G. Cain, E. Vallejo, D. Ellis, and F. Mendels, "Dynamic properties of AFM cantilevers and the calibration of their spring constants," *J. Micromech. Microeng.*, vol. 16, no. 8, pp. 1720–1733, 2006.
- [33] D. Sarid, *Scanning Force Microscopy*. Oxford, U.K.: Oxford Univ. Press, 1991.
- [34] J. Colchero, H. Bielefeldt, A. Ruf, M. Hipp, O. Marti, and J. Mlynek, "Scanning force and friction microscopy," *Phys. Stat. Sol. A*, vol. 131, no. 1, pp. 73–75, 1992.
- [35] T. E. Schaffer and P. R. Hansma, "Characterization and optimization of the detection sensitivity of an atomic force microscope for small cantilevers," *J. Appl. Phys.*, vol. 84, no. 9, pp. 4661–4666, Nov. 1, 1998.
- [36] L. Y. Beaulieu, M. Godin, O. Laroche, V. Tabard-Cossa, and P. Grütter, "Calibrating laser beam deflection systems for use in atomic force microscopes and cantilever sensors," *Appl. Phys. Lett.*, vol. 88, no. 8, pp. 083108–1083108, 2006.
- [37] T. E. Schaffer and P. R. Hansma, "Characterization and optimization of the detection sensitivity of an atomic force microscope for small cantilevers," *J. Appl. Phys.*, vol. 84, no. 9, pp. 4661–4666, Nov. 1, 1998.



Associate in December 2006. His main research interests include micro-robotics/nanorobotics, microscopy vision, system design, and implementation.



Julien Vitard received the M.S. degree (French DEA) in virtual reality and complex systems control from the University of Evry and INSTN (Saclay CEA), Paris, France, in 2004. He is currently pursuing the Ph.D. degree in mechanics and robotics from the University of Pierre & Marie Curie, Paris, in 2008.

His research interests are micro and nano characterization/manipulation from robotics and physics approaches.



Dogan Sinan Haliyo was born in Istanbul in 1976. He received the Ph.D. degree in robotics in 2002 from the University of Pierre & Marie Curie, Paris, France.

He has been an Associate Professor with the Institute of Intelligent Systems and Robotics (ISIR), University of Pierre & Marie Curie, since 2005. His main interests are in micro and nanomanipulation and related topics such as microscale phenomena, remote handling, and biology-driven self-assembly.



Stéphane Régnier received the Ph.D. degree in mechanics and robotics from the University of Pierre & Marie Curie, Paris, France, in 1996.

He is currently an Associate Professor with the Institute of Intelligent Systems and Robotics (ISIR), University of Pierre & Marie Curie, Paris, France. He has been Head of the Micromanipulation Team, ISIR, since 2001. His research interests are focused on micro and nano manipulation, teleoperation, and haptic feedback at the nanoscale, micromechanics, and biological cell characterization.